

# Neutron star deformation due to multipolar magnetic fields

A. Mastrano<sup>\*</sup>, P. D. Lasky<sup>†</sup>, and A. Melatos<sup>‡</sup>  
*School of Physics, University of Melbourne, Parkville VIC 3010, Australia*

Accepted ?. Received ?; in original form ?

## ABSTRACT

Certain multi-wavelength observations of neutron stars, such as intermittent radio emissions from rotation-powered pulsars beyond the pair-cascade death line, the pulse profile of the magnetar SGR 1900+14 after its 1998 August 27 giant flare, and X-ray spectral features of PSR J0821–4300 and SGR 0418+5729, suggest that the magnetic fields of non-accreting neutron stars are not purely dipolar and may contain higher-order multipoles. Here, we calculate the ellipticity of a non-barotropic neutron star with (i) a quadrupole poloidal-toroidal field, and (ii) a purely poloidal field containing arbitrary multipoles, deriving the relation between the ellipticity and the multipole amplitudes. We present, as a worked example, a purely poloidal field comprising dipole, quadrupole, and octupole components. We show the correlation between field energy and ellipticity for each multipole, that the  $l = 4$  multipole has the lowest energy, and that  $l = 5$  has the lowest ellipticity. We show how a mixed multipolar field creates an observationally testable mismatch between the principal axes of inertia (to be inferred from gravitational wave data) and the magnetic inclination angle. Strong quadrupole and octupole components (with amplitudes  $\sim 10^2$  times higher than the dipole) in SGR 0418+5729 still yield ellipticity  $\sim 10^{-8}$ , consistent with current gravitational wave upper limits. The existence of higher multipoles in fast-rotating objects (e.g., newborn magnetars) has interesting implications for the braking law and hence phase tracking during coherent gravitational wave searches.

**Key words:** MHD – stars: magnetic field – stars: interiors – stars: neutron – gravitational waves

## 1 INTRODUCTION

Neutron star magnetic fields are approximately dipolar at (i) radio emission altitudes [leading to S-shaped radio polarization swings (Lyne & Manchester 1988; Chung & Melatos 2011; Burnett & Melatos 2013) and the pulse-width-period relation (Rankin 1993)] and (ii) in the outer magnetosphere, where high-energy emission is produced (Romani & Yadigaroglu 1995; Lyutikov, Otte, & McCann 2012). For millisecond pulsars, Arons (1993) calculated the surface strength of non-dipolar components to be  $\lesssim 40\%$  of the dipole. However, some observations, such as the anomalous braking index of some radio pulsars (Barsukov & Tsygan 2010), intermittent radio emission from pulsars beyond the pair-cascade ‘death line’ (Young, Manchester, & Johnston 1999; Camilo et al. 2000; Gil & Mitra 2001; McLaughlin et al. 2003; Medin & Lai 2010),<sup>1</sup> cyclotron resonant scattering line energies of some accretion-powered X-ray pulsars (Nishimura 2005), the pulse profile of SGR 1900+14 following its 1998 August 27 giant flare (Feroci et al. 2001; Thompson & Duncan 2001; Thompson, Lyutikov, & Kulkarni 2002), and X-ray spectral features of PSR J0821–4300 (Gotthelf, Halpern, & Alford 2013) and SGR 0418+5729 (Güver, Özel F., & Göğüş 2011; Güver, Göğüş, & Özel 2011), have been taken to indicate the presence of higher-order multipoles close to the surface.

<sup>\*</sup> E-mail: alpham@unimelb.edu.au

<sup>†</sup> E-mail: paul.lasky@unimelb.edu.au

<sup>‡</sup> E-mail: amelatos@unimelb.edu.au

<sup>1</sup> An alternative explanation for these pulsars beyond the death line involves an ‘offset’ dipole, see Arons (2000), Burnett & Melatos (2013), and references therein. We do not consider the offset dipole model in this paper.

Furthermore, while the external magnetic field of a neutron star is readily inferred from its spin-down rate, its internal field is not directly observable and may be composed of high-order multipoles too. Activity in magnetars, e.g., giant flares from soft gamma-ray repeaters (SGRs), has been interpreted to imply the existence of a strong, readjusting internal magnetic field (Ioka 2001), and simulations indicate that this internal field may be in a ‘twisted torus’ configuration (Braithwaite & Nordlund 2006; Braithwaite & Spruit 2006). In previous papers (Mastrano et al. 2011; Mastrano & Melatos 2012), we showed how gravitational wave observations constrain the internal field strength. In this paper, we discuss the effects of non-dipolar geometries on the deformation of neutron stars and, hence, their gravitational wave emission.

It is well known that a magnetic field deforms a star (Chandrasekhar & Fermi 1953; Ferraro 1954; Goossens 1972; Katz 1989; Payne & Melatos 2004; Haskell et al. 2008; Mastrano et al. 2011). Neutron stars, with their intense fields, therefore possess significant ellipticities under certain circumstances, making them good candidates for gravitational wave sources (Bonazzola & Gourgoulhon 1996; Melatos & Payne 2005; Stella et al. 2005; Haskell et al. 2008; Dall’Osso et al. 2009). Observational upper limits from gravitational waves can be used to set upper limits on stellar ellipticity. Ellipticity, which is roughly proportional to the magnetic energy (Cutler 2002; Haskell et al. 2008; Dall’Osso et al. 2009), can thus be used to constrain the strength and topology of a star’s internal field (Cutler 2002; Dall’Osso et al. 2009; Abbott et al. 2010; Mastrano et al. 2011; Pitkin 2011).

Mastrano et al. (2011) constructed hydromagnetic equilibria for stratified, non-barotropic stars. The barotropic assumption restricts the forms of the poloidal and toroidal components that can be ‘fitted’ into the star. Haskell et al. (2008) found that the field must vanish at the surface, contrary to observations, and Lander & Jones (2009) and Cioffi, Ferrari, & Gualtieri (2010) found that only configurations dominated by the poloidal component (poloidal energy  $\gtrsim 90\%$  of total) are allowed, contrary to numerical simulations of magnetic field evolution [e.g., Braithwaite & Nordlund (2006)]. By abandoning the barotropic assumption, and assuming stable radial stratification (Pethick 1992; Reisenegger & Goldreich 1992; Reisenegger 2009; Akgün et al. 2013), Mastrano et al. (2011) were able to construct a simple, self-consistent hydromagnetic equilibrium, with an internal field that can be matched to an external dipole (so it can be related directly to observations of the external field), keeping the relative strengths of the poloidal and toroidal components independently adjustable. A purely poloidal (Markey & Tayler 1973; Wright 1973) or a purely toroidal (Tayler 1973) magnetic field is unstable, but theoretical calculations and numerical simulations (Braithwaite & Nordlund 2006) suggest that a magnetic field with both poloidal and toroidal components is stable over dissipative time-scales (i.e., much longer than the Alfvén time-scale). Because a non-barotropic star allows arbitrary poloidal and toroidal field strengths, it can easily accommodate the strong internal fields which, as suggested by the numerical simulations of Braithwaite & Nordlund (2006), are required to stabilise the star.

In this paper, we show how the ellipticity calculation of Mastrano et al. (2011) can be generalised to higher multipoles. An axisymmetric magnetic field of a particular configuration is chosen, the density perturbation induced by this field is calculated, and the ellipticity is calculated from the density perturbation. We show how, in principle, gravitational wave observations constrain the relative strengths of the internal magnetic multipoles. In Sec. 2, we briefly describe how the unmagnetised hydrostatic equilibrium state is chosen and how the density perturbation is calculated. In Sec. 3, we recap briefly the results of Mastrano et al. (2011) for a dipole poloidal-plus-toroidal magnetic field and show how the analysis can be extended to add an axisymmetric quadrupole. In Sec. 4, we generalize the work of Mastrano et al. (2011) to any purely poloidal, axisymmetric magnetic field. We illustrate the general theory by calculating explicitly the ellipticity of a star with mixed dipole, quadrupole, and octupole poloidal fields. Lastly, in Sec. 5, we summarize our results and discuss how to constrain the relative weighting of multipoles from current gravitational wave upper limits and future gravitational wave detections.

## 2 GENERAL FORMALISM

In the absence of a magnetic field, the star is spherically symmetric and in hydrostatic equilibrium. Let  $(r, \theta, \phi)$  be spherical polar coordinates, with  $r$  expressed in units of the stellar radius  $R_*$ , so that it is dimensionless. To make contact with previous work (Mastrano et al. 2011; Mastrano & Melatos 2012), we adopt the idealised density profile

$$\rho = \rho_c(1 - r^2), \quad (1)$$

where  $\rho_c = 15M_*/(8\pi R_*^3)$  is the density at the centre, and  $M_*$  is the stellar mass. We emphasize that this is a particular, simple choice of density profile, chosen to render the following calculations tractable, rather than motivated directly by observations or the theory of stellar structure, but it does approximate the  $n = 1$  polytrope reasonably well (Mastrano et al. 2011).

Any axisymmetric magnetic field can be written as (Chandrasekhar 1956)

$$\mathbf{B} = B_0[\eta_p \nabla \alpha(r, \theta) \times \nabla \phi + \eta_t \beta(r, \theta) \nabla \phi], \quad (2)$$

where  $B_0$  is the surface field strength at the equator, and  $\eta_p$  and  $\eta_t$  are dimensionless parameters defining the relative strengths of the poloidal and toroidal components respectively. The stream function  $\alpha(r, \theta)$  can always be factorised into radial and

polar parts, i.e.,  $\alpha(r, \theta) = f(r)\Theta(\theta)$ . In addition, the scalar function  $\beta$  must be a function of  $\alpha$ , so that the magnetic force  $[\propto (\nabla \times \mathbf{B}) \times \mathbf{B}]$  does not have an azimuthal component, which cannot be balanced in hydromagnetic equilibrium.

The magnetic energy density is  $\lesssim 10^{-6}$  of the gravitational energy density and hence the pressure  $p$ . Even in a magnetar, the magnetic force on the star can be treated as a perturbation on a background hydrostatic equilibrium. Thus, we write the hydromagnetic force balance equation as<sup>2</sup>

$$\frac{1}{\mu_0}(\nabla \times \mathbf{B}) \times \mathbf{B} = \nabla \delta p + \delta \rho \nabla \Phi, \quad (3)$$

to first order in  $B^2/(\mu_0 p)$  and in the Cowling approximation ( $\delta \Phi = 0$ , where  $\Phi$  is the gravitational potential). Note that we do *not* require the density perturbation  $\delta \rho$  to be a function purely of the pressure perturbation  $\delta p$  (the barotropic assumption). Therefore, we do not restrict the relative strengths of the poloidal and toroidal components of the magnetic field. We only require the following properties:

- (i) the field is cylindrically symmetric about the  $z$ -axis;
- (ii) the poloidal component is continuous with a purely poloidal field outside the star (so there are no surface currents);
- (iii) the toroidal component is confined to some region inside the star (since the external field has no toroidal component);
- (iv) the current density remains finite and continuous everywhere in the star and vanishes at the surface (since we assume the external field to exist in vacuo, neglecting magnetospheric currents).

All these requirements can be satisfied by choosing a suitable  $\alpha$ .

This approach differs from that taken by previous authors (Haskell et al. 2008; Lander & Jones 2009; Ciolfi, Ferrari, & Gualtieri 2010), who pre-specified a barotropic equilibrium model and then solved for the magnetic field configuration. Because our star is non-barotropic, i.e., because density (background plus perturbation) is not purely a function of pressure, our magnetic field is not constrained by the stellar equation of state, and the toroidal and poloidal components are separately adjustable [they do not need to obey any relations to ensure  $\delta \rho = \delta \rho(\delta p)$ ]. In other words, we stipulate the form of the magnetic field we wish to investigate (eventually to be determined from observational constraints) and solve for the neutron star structure (strictly speaking, the part controlling the ellipticity) that accommodates it. No particular physical stratification mechanism is specified; it is assumed to be whatever is needed to accommodate the chosen field.

We characterize the magnetic deformation of the star by its ellipticity  $\epsilon$ , defined as

$$\epsilon = \frac{I_{zz} - I_{xx}}{I_0}, \quad (4)$$

where  $I_0$  is the moment of inertia of the spherical star, and the moment-of-inertia tensor is given by

$$I_{jk} = R_*^5 \int d^3 \mathbf{x} [\rho(r) + \delta \rho(r, \theta)] (r^2 \delta_{jk} - x_j x_k), \quad (5)$$

with the integral covering the interior,  $r \leq 1$ .

We calculate  $\delta \rho$  by taking the curl of both sides of Eq. (3). Matching the  $\phi$  components, we find

$$\frac{\partial \delta \rho}{\partial \theta} = -\frac{r}{\mu_0 R_*} \frac{dr}{d\Phi} \{ \nabla \times [(\nabla \times \mathbf{B}) \times \mathbf{B}] \}_\phi. \quad (6)$$

Given  $\mathbf{B}$ , Eq. (6) can be integrated up to an arbitrary function of  $r$  (which does not contribute to the ellipticity). Equations (4)–(5) are subsequently evaluated to give  $\epsilon$ .

### 3 POLOIDAL-TOROIDAL FIELDS

In this section, we briefly review the results of Mastrano et al. (2011) for a dipole-plus-toroidal field (Sec. 3.1). Then we apply the same method to calculate  $\epsilon$  for a poloidal-toroidal field with a quadrupole poloidal component (Sec. 3.2).

#### 3.1 Dipole plus toroidal field

Mastrano et al. (2011) considered dipole poloidal-plus-toroidal magnetic field configurations. Such fields are broadly representative of the output of numerical simulations (Braithwaite & Nordlund 2006; Braithwaite & Spruit 2006; Braithwaite 2009). The poloidal flux function is taken to be  $\alpha_1 = f_1(r) \sin^2 \theta$ , so that continuity of the poloidal component with an external dipole

<sup>2</sup> Throughout this paper, we use SI units: 1 T =  $10^4$  G.

field is ensured.<sup>3</sup> The function  $f_1(r)$  is arbitrary, in principle. For simplicity, Mastrano et al. (2011) assumed a polynomial in  $r$ . One possible choice is  $f_1(r) = (35/8)[r^2 - (6/5)r^4 + (3/7)r^6]$ , ensuring that all the continuity and regularity conditions for the field and current in Sec. 2 are fulfilled.<sup>4</sup> The toroidal flux function is chosen to be  $\beta_1(\alpha_1) = (\alpha_1 - 1)^2$  for  $\alpha_1 \geq 1$  and  $\beta_1(\alpha_1) = 0$  elsewhere, so that the toroidal field is confined to the region around the neutral line, where  $\alpha_1$  exceeds unity.

Following the procedure in Sec. 2, the ellipticity is calculated to be (Mastrano et al. 2011; Mastrano & Melatos 2012)

$$\epsilon_1 = 5.63 \times 10^{-6} \left( \frac{B_{\max}}{10^{11} \text{T}} \right)^2 \left( \frac{M_*}{1.4 M_\odot} \right)^{-2} \left( \frac{R_*}{10^4 \text{m}} \right)^4 \left( 1 - \frac{0.351}{\Lambda} \right), \quad (7)$$

where  $\Lambda$  is the ratio of the poloidal component's energy to the total magnetic energy<sup>5</sup> ( $\Lambda = 0$  is a purely toroidal field and  $\Lambda = 1$  is purely poloidal), and  $B_{\max}$  is the maximum surface field strength (i.e., at the poles). Note that we work in SI units,  $1 \text{ T} = 10^4 \text{ G}$ ,  $1 \text{ J} = 10^7 \text{ ergs}$ .<sup>6</sup> In previous papers, Eq. (7) was combined with gravitational wave upper limits to place bounds on  $\Lambda$  for the Crab pulsar, the Cassiopeia A central compact object, newly born magnetars in the Virgo cluster (Mastrano et al. 2011), and millisecond pulsars (Mastrano & Melatos 2012).

### 3.2 Quadrupole-poloidal-plus-equatorial-toroidal field

We now calculate the ellipticity due to a mixed poloidal-toroidal field, where the poloidal component is a quadrupole and the toroidal component remains the same as in Sec. 3.1 (localised around the equator). Pulsar observations tell us that neutron star magnetic fields are largely dipolar (Chung & Melatos 2011), but we assume that the poloidal component is purely quadrupolar as a first step, in order to understand the effects of higher multipoles on  $\epsilon$ . Outside the star, the field takes the following form:

$$\mathbf{B}_{\text{ext}} = \frac{B_0}{r^4} [(3 \cos^2 \theta - 1) \hat{\mathbf{e}}_r - 2 \sin \theta \cos \theta \hat{\mathbf{e}}_\theta]. \quad (8)$$

In order to express the field in the form given by Eq. (2), the poloidal flux function must take the form of

$$\alpha_2 = f_2(r) \sin^2 \theta \cos \theta. \quad (9)$$

Following Sec. 3.1, suppose  $f_2(r)$  is a polynomial. As before, we must first ensure that the current

$$\nabla \times \mathbf{B} \propto \left( \frac{f_2''}{r} - \frac{6f_2}{r^3} \right) \sin \theta \cos \theta \quad (10)$$

is well-behaved as  $r \rightarrow 0$ , requiring the polynomial to be of degree three or higher. Next, we must ensure that the normal and tangential components of the field and the current are continuous at  $r = 1$ . Therefore, we need at least three terms in the polynomial. We find that  $f_2(r) = 21(r^3 - \frac{5}{3}r^4 + \frac{5}{7}r^5)$  satisfies all the conditions, implying

$$\mathbf{B}_2 = \begin{cases} 21\eta_p B_0 [(r - \frac{5}{3}r^2 + \frac{5}{7}r^3) (3 \cos^2 \theta - 1) \hat{\mathbf{e}}_r - (3r - \frac{20}{3}r^2 + \frac{25}{7}r^3) \sin \theta \cos \theta \hat{\mathbf{e}}_\theta] + \frac{\eta_t B_0 \beta_2(\alpha_2) \hat{\mathbf{e}}_\phi}{r \sin \theta} & \text{for } r < 1 \\ \eta_p B_0 r^{-4} [(3 \cos^2 \theta - 1) \hat{\mathbf{e}}_r + 2 \sin \theta \cos \theta \hat{\mathbf{e}}_\theta] & \text{for } r \geq 1. \end{cases} \quad (11)$$

Again, following Sec. 3.1, we choose the toroidal flux function to be

$$\beta_2(\alpha_2) = \begin{cases} (|\alpha_2| - 1)^2 & \text{for } \alpha_1 \geq 1 \\ 0 & \text{for } \alpha_1 < 1. \end{cases} \quad (12)$$

Equation (12) confines the toroidal component to the region near the equator that would be occupied by the toroidal component of a dipole field (see Sec. 3.1), instead of to the region around the neutral curves of the quadrupole poloidal field itself, located at  $\theta = \cos^{-1}(\pm \sqrt{1/3})$ . This is because we expect the toroidal magnetic field generated and/or amplified by differential rotation in a newly born neutron star to be strongest near the equator (Braithwaite & Nordlund 2006; Rezzolla et al. 2001a,b). We do not suggest here that a neutron star's internal field is predominantly a quadrupole plus a toroidal field at the equator. Indeed, simulations typically generate dipole-dominated configurations (Braithwaite & Nordlund 2006; Rezzolla et al. 2001a,b). Here, we simply wish to investigate the effects of a quadrupole poloidal component together with some well-motivated toroidal component, and we cite the aforementioned simulations to justify placing the toroidal component at the equator. Furthermore, we find that reasonably simple forms for  $\beta_2$  with toroidal field components located around the quadrupole's neutral curves

<sup>3</sup> Anticipating Sec. 4, where we discuss arbitrary multipoles, we label all variables with a subscript denoting multipole number  $l$ .

<sup>4</sup> We discuss briefly the possibility of a four-term polynomial for  $f(r)$  in Appendix A.

<sup>5</sup> Magnetic energies are implicitly taken to be *internal*; i.e., we integrate  $\mathbf{B}^2$  only to the surface of the star.

<sup>6</sup> The lead author apologizes for this cherished idiosyncrasy, which Lasky and Melatos do not share as strongly.

lead to unphysical, discontinuous  $\delta\rho$ , because the magnetic force that induces  $\delta\rho$  is not symmetric about  $\theta = \cos^{-1}(\pm\sqrt{1/3})$  [at least for simple forms of  $\beta_2$ , e.g., a polynomial in  $\alpha_2$  as given by Eq. (12)], making it impossible for  $\delta\rho$  to vanish smoothly at the torus boundary. We defer the derivation of a quadrupole toroidal field which is mathematically consistent to a future paper.

We sketch the field lines of the dipole in the left-hand panel and those of the quadrupole in the right-hand panel of Fig. 1. The toroidal field fills the region enclosed by the black dotted curve. In the left-hand panel, the toroidal region is centred around the neutral curve and is bounded by the last dipole field line that fully closes inside the star. The quadrupole (right-hand panel) has one neutral curve in each hemisphere. As stated above, however, since a toroidal magnetic field generated and amplified by differential rotation near the equator is more physically compelling (Braithwaite & Nordlund 2006; Rezzolla et al. 2001a,b), we choose to confine the toroidal field to the same region as in Sec. 3.1, defined by  $|\alpha_1| \leq 1$  (instead of the closed quadrupole field lines around the neutral curves).

Upon evaluating Eqs. (4), (5), (11), and (12), we obtain

$$\epsilon_2 = 1.84 \times 10^{-6} \left( \frac{B_{\max}}{10^{11}\text{T}} \right)^2 \left( \frac{M_*}{1.4M_\odot} \right)^{-2} \left( \frac{R_*}{10^4\text{m}} \right)^4 \left( 1 - \frac{0.359}{\Lambda} \right), \quad (13)$$

where  $B_{\max}$  is the maximum surface field strength (i.e., the surface field strength at the poles). The dependence on  $\Lambda$  is similar to the dipole case [Eq. (7)], because the toroidal field is confined to the same region as before. If the toroidal field is localised elsewhere (e.g., around the neutral curves of the quadrupole), the dependence of  $\epsilon$  on  $\Lambda$  changes. In addition, for given  $B_{\max}$ ,  $M_*$ , and  $R_*$ , the quadrupole deforms the star less than the dipole, i.e.  $|\epsilon_2| < |\epsilon_1|$ , because the magnetic energy of a quadrupole is less than for a dipole with the same  $B_{\max}$ .

## 4 COMPOSITE POLOIDAL FIELDS

In this section, we discuss neutron star deformation due to a field that is a superposition of multipoles. First, in Sec. 4.1, we derive a general formula for  $\epsilon$  due to a multipole of order  $l$ . Then, in Sec. 4.2, we calculate  $\epsilon$  due to a purely poloidal, composite dipole-plus-quadrupole-plus-octupole field as a worked example.

### 4.1 General formula for $\epsilon$

Let us calculate  $\epsilon$  for any purely poloidal field that is a superposition of axisymmetric multipoles. We describe the field in terms of spherical harmonics  $Y_{lm}(\theta, \phi)$ , with  $\mathbf{B} = \sum_l \eta_l \mathbf{B}_l$  ( $l \geq 1$ ) and

$$\mathbf{B}_l = B_0 [g_l(r) Y_{l0}(\theta) \hat{\mathbf{e}}_r + h_l(r) Y'_{l0}(\theta) \hat{\mathbf{e}}_\theta]. \quad (14)$$

Here,  $\eta_l$  are constants that determine the weighting of the components, and the prime denotes a derivative with respect to  $\theta$ .

The radial functions  $g_l(r)$  and  $h_l(r)$  must be determined for each multipole, such that the conditions in Sec. 2 are fulfilled. Because the spherical harmonics form an orthonormal basis, the total field automatically fulfills the conditions if each multipole fulfills the conditions separately. The task of determining  $g_l(r)$  and  $h_l(r)$  is made easier by the fact that, according to Eq. (2),  $g_l$  and  $h_l$  are related through some stream function  $\alpha(r, \theta) = f(r)\Theta(\theta)$ . By comparing Eq. (14) and the poloidal part of Eq. (2), we find that each multipole obeys  $g_l = l(l+1)f/r^2$ ,  $h_l = f'/r$ ,  $\Theta'(\theta) = Y_{l0}(\theta)l(l+1)\sin\theta$ , and  $\Theta(\theta) = -Y'_{l0}(\theta)\sin\theta$ . The field always takes its maximum value,  $B_{\max} = [(l+1)^2(2l+1)/(4\pi)]^{1/2}B_0$ , at the poles.

The current density associated with each multipole is

$$\mu_0^{-1} \nabla \times \mathbf{B} = \mu_0^{-1} B_0 \left[ \frac{f''}{r} - l(l+1) \frac{f}{r^3} \right] Y_{l0} \hat{\mathbf{e}}_\phi. \quad (15)$$

The polynomial  $f(r)$  must contain terms of certain orders if the current is to be well-behaved at the origin;  $f(r)$  must also contain at least three terms to fulfill the three conditions at  $r = 1$  (cf. Appendix A). For the quadrupole, the terms  $r^3$ ,  $r^4$ , and  $r^5$  are sufficient. For the octupole and higher-order multipoles, the terms  $r^4$ ,  $r^5$ , and  $r^6$  are sufficient. We solve for their coefficients from the following boundary conditions at  $r = 1$ :  $f''(1) - l(l+1)f(1) = 0$ ;  $lf(1) = -1$ ; and  $f'(1) = 1$ . As noted in Sec. 2, the conditions ensure that the current vanishes at the surface and that the magnetic field is continuous there (i.e., zero surface current).

Upon substituting Eq. (14) into Eq. (6) and integrating, we obtain

$$\frac{-\mu_0 R_*}{B_0^2} \left( \frac{d\Phi}{dr} \right) \delta\rho = \sum_l \sum_k \frac{\eta_l \eta_k}{r} \left[ \frac{d(rh_l)}{dr} - g_l \right] h_k Y'_{l0}(\theta) Y'_{k0}(\theta) + \eta_l \eta_k \frac{d}{dr} \left\{ \left[ \frac{d(rh_l)}{dr} - g_l \right] g_k \right\} \int^\theta d\theta' Y'_{l0}(\theta') Y_{k0}(\theta'), \quad (16)$$

where the last integral is an indefinite integral of  $Y'_{l0}(\theta')Y_{k0}(\theta')$  over the dummy variable  $\theta'$ . Strictly speaking, an arbitrary

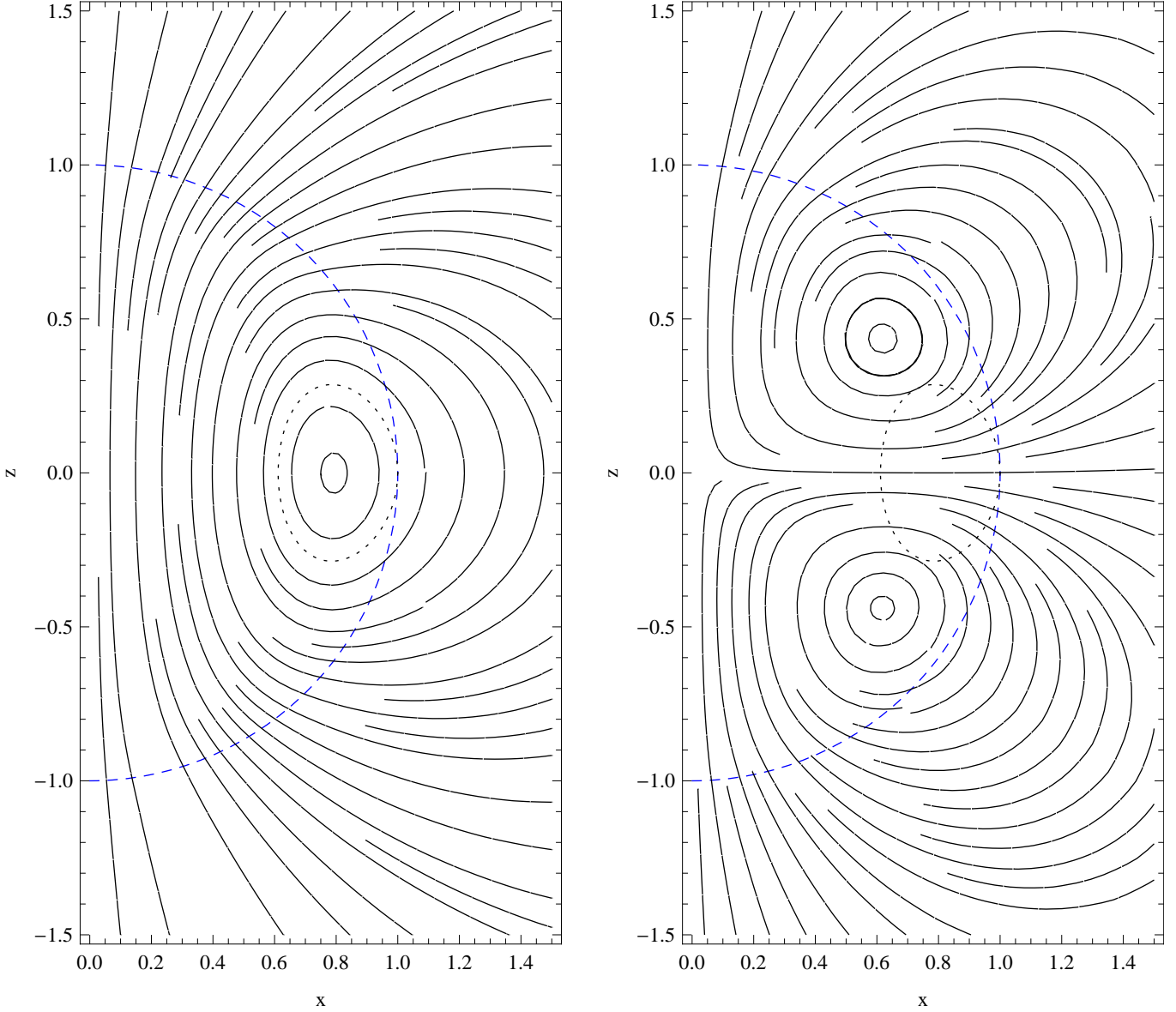


**Figure 1.** Magnetic field lines for a dipole (left) and a quadrupole (right). The surface of the star is represented by the blue dashed semicircle. The toroidal field component is confined to the region bounded by the black dotted curve and fills a torus around the  $z$ -axis. Apparent discontinuities in the field lines are plotting artifacts. The dipole field is north-south antisymmetric, and the quadrupole is north-south symmetric. Also, the dipole only has one neutral curve (where the poloidal field vanishes) at the equator, but the quadrupole has two, located at  $\theta = \cos^{-1}(\pm\sqrt{1/3})$ .

function of  $r$  can be added to  $\delta\rho$ , but it does not alter the mass quadrupole moment, which is the focus of the paper. Substituting  $\delta\rho$  from Eq. (16) into Eq. (5), we obtain

$$\epsilon = -\frac{B_0^2 R_*^4}{4\mu_0 I_0} \sum_{l=1}^{l_{\max}} \sum_{k=1}^{k_{\max}} \eta_l \eta_k \sqrt{(2l+1)(2k+1)} (\epsilon_{a,lk} + \epsilon_{b,lk}), \quad (17)$$

with

$$\epsilon_{a,lk} = \int_{-1}^1 dx P_l'(x) P_k'(x) (1-x^2)(1-3x^2) \int_0^1 dr \left( \frac{dr}{d\Phi} \right) r^3 \left[ \frac{d(rh_l)}{dr} - g_l \right] h_k, \quad (18)$$

$$\epsilon_{b,lk} = \int_{-1}^1 dx \left[ \int_{-x}^x dy P_l(y) P_k'(y) \right] (1-3x^2) \int_0^1 dr \left( \frac{dr}{d\Phi} \right) r^4 \frac{d}{dr} \left\{ \left[ \frac{d(rh_l)}{dr} - g_l \right] g_k \right\}, \quad (19)$$

where  $P_l(x) = (2^l l!)^{-1} d^l(x^2-1)^l/dx^l$  is the Legendre polynomial of order  $l$ . There are no cross terms between the multipoles in  $(\nabla \times \mathbf{B}) \times \mathbf{B}$  (i.e., both  $\epsilon_{a,lk}$  and  $\epsilon_{b,lk}$  vanish when  $l \neq k$ ), except between  $l$  and  $l \pm 2$ . For example, this means that, if the field consists only of a dipole and a quadrupole, each multipole can be treated separately, and the total force and  $\epsilon$  are simple sums of the individual contributions.

To understand the correlation between  $\epsilon$  and magnetic energy, we first relate the weights  $\eta_l$  to  $B_{\max}$  and to the total magnetic energy. Magnetic field energy is defined to be

$$E = \int_{r \leq 1} dV \frac{\mathbf{B}^2}{2\mu_0} = \sum_l E_l, \quad (20)$$

where the energy in the  $l$ -th multipole is

$$E_l = \frac{2\pi R_*^3 B_{l,\max}^2}{(2l+1)(l+1)^2 \mu_0} \int_0^1 dr r^2 [g_l^2 + l(l+1)h_l^2], \quad (21)$$

and  $B_{l,\max}$  is the maximum surface field strength of that multipole. If  $g_l$  and  $h_l$  are polynomials with three terms in  $r$  (to satisfy the three boundary conditions in Sec. 2), it can be shown by explicit calculation that the polynomials with the lowest allowed orders that satisfy the conditions in Sec. 2 (i.e., a polynomial with  $r^3$ ,  $r^4$ , and  $r^5$  terms for the quadrupole and a polynomial with  $r^4$ ,  $r^5$ , and  $r^6$  terms for octupole and higher) maximise  $E_l$ . We therefore assume throughout the rest of the paper that  $g_l$  and  $h_l$  are three-term polynomials with the lowest allowed orders.

In Fig. 2, we plot the magnetic energy and  $\epsilon$  for single-multipole fields as functions of multipole order  $l$ , for a star of mass  $1.4M_\odot$ , radius  $10^4$  m, and  $B_{l,\max} = 10^{11}$  T. We see that  $\epsilon$  is generally proportional to  $E$ , and that, for a given  $B_{l,\max}$ , stellar mass, and radius,  $l = 4$  has the lowest energy and  $l = 5$  has the lowest  $\epsilon$ ;  $E$  increases monotonically for  $l > 4$ , and  $\epsilon$  increases monotonically for  $l > 5$ .

## 4.2 Worked example: dipole plus quadrupole plus octupole

To illustrate the theory in Sec. 4.1, let us evaluate the specific case  $\mathbf{B} = \sum_{l=1}^3 \eta_l \mathbf{B}_l$ , i.e., a superposition of purely poloidal dipole, quadrupole, and octupole components. For the dipole, quadrupole, and octupole field energies, we find

$$E_1 = \frac{59}{33} \frac{\pi B_{1,\max}^2 R_*^3}{\mu_0}, \quad (22)$$

$$E_2 = \frac{31}{30} \frac{\pi B_{2,\max}^2 R_*^3}{\mu_0}, \quad (23)$$

$$E_3 = \frac{449}{770} \frac{\pi B_{3,\max}^2 R_*^3}{\mu_0}. \quad (24)$$

Now let us calculate  $\epsilon$  for a linear superposition of  $l = 1, 2, 3$  multipoles. From Eq. (14) and Eqs. (18)–(20), after some algebra, we find

$$\epsilon = 3.65 \times 10^{-6} \left( \frac{B_{1,\max}}{10^{11} \text{T}} \right)^2 \left( \frac{M_*}{1.4M_\odot} \right)^{-2} \left( \frac{R_*}{10^4 \text{m}} \right)^4 \left[ 1 + a_1 \left( \frac{E_3}{E_1} \right)^{1/2} + \frac{a_2 E_3}{E_1} + \frac{a_3 E_2}{E_1} \right], \quad (25)$$

with  $a_1 = 2.426$ ,  $a_2 = 0.567$ , and  $a_3 = 0.559$ . There are no cross terms between  $l = 1$  and  $l = 2$ , so the contribution of the quadrupole to the total  $\epsilon$  is a simple linear term.

For situations where the total magnetic energy  $E_{\text{tot}}$  is known (e.g., constrained using SGR giant flare observations), we express  $\epsilon$  in terms of  $E_2/E_{\text{tot}}$  and  $E_3/E_{\text{tot}}$ :

$$\epsilon = 4.64 \times 10^{-7} \left( \frac{E_{\text{tot}}}{10^{40} \text{J}} \right) \left( \frac{M_*}{1.4M_\odot} \right)^{-2} \left( \frac{R_*}{10^4 \text{m}} \right) \left[ 1 + b_1 \left( 1 - \frac{E_2}{E_{\text{tot}}} - \frac{E_3}{E_{\text{tot}}} \right) + b_2 \left( 1 - \frac{E_2}{E_{\text{tot}}} - \frac{E_3}{E_{\text{tot}}} \right)^{1/2} \left( \frac{E_3}{E_{\text{tot}}} \right)^{1/2} + \frac{b_3 E_2}{E_{\text{tot}}} \right], \quad (26)$$

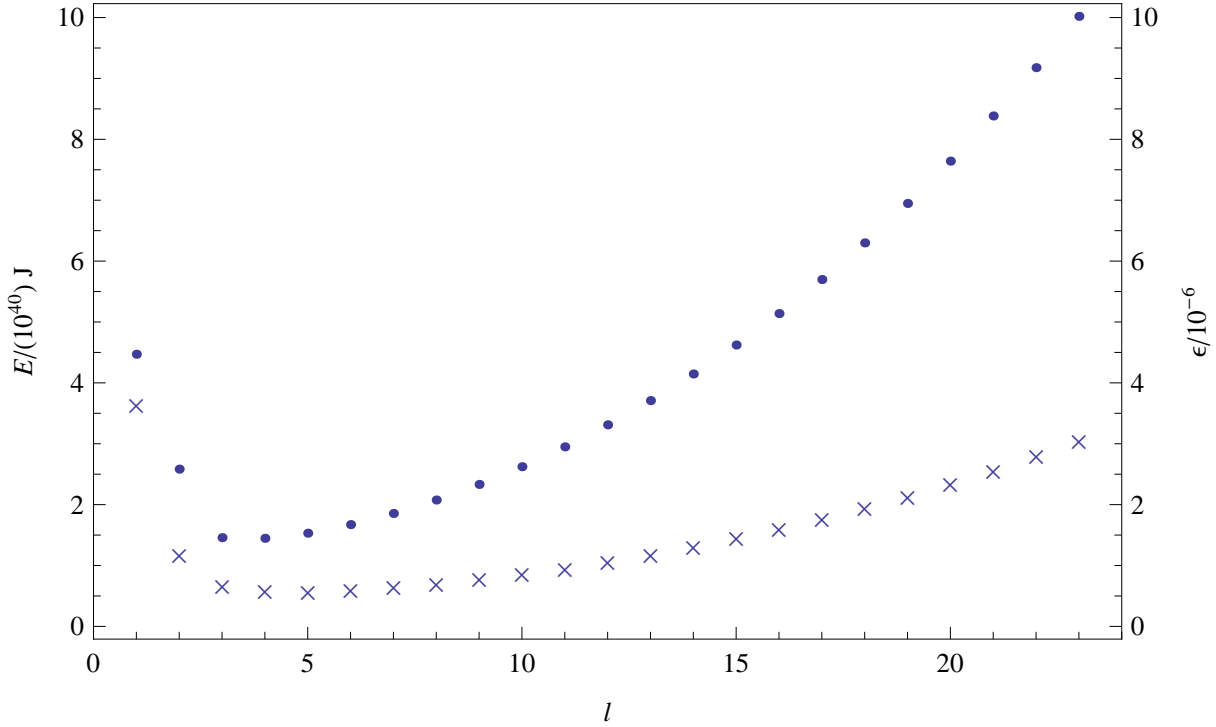


**Figure 2.** Magnetic energy  $E_l$  (dots, left axis) and ellipticity  $\epsilon$  (crosses, right axis) for purely poloidal multipoles, considered separately, as functions of the multipole order  $l$ . We assume that the star has mass  $M_* = 1.4M_\odot$ , radius  $10^4$  km, and  $B_{l,\max} = 10^{11}$  T. Ellipticity is directly proportional to  $B_{l,\max}^2 R_*^4$  and inversely proportional to  $M_*^2$ .

with  $b_1 = 0.762$ ,  $b_2 = 4.275$ , and  $b_3 = -1.526 \times 10^{-2}$ . We plot field lines for some representative combinations of  $E_2/E_{\text{tot}}$  and  $E_3/E_{\text{tot}}$  in Fig. 3. The pure multipoles are north-south symmetric or antisymmetric, so a superposition of even (odd) multipoles is always symmetric (antisymmetric), for example, (0.0, 1.0) and (0.0, 0.8) in Fig. 3. However, when odd and even multipoles are mixed, the  $\theta$ -dependence of the field is no longer (anti)symmetric about the equator, for example, (0.5, 0.5) and (0.2, 0.6) in Fig. 3.

In Fig. 4, we plot  $\epsilon$  as a function of  $E_3/E_1$  for selected values of  $E_2/E_1$  (left-hand panel, for  $B_{1,\max} = 10^{11}$  T) and as a function of  $E_3/E_{\text{tot}}$  for selected values of  $E_2/E_{\text{tot}}$  (right-hand panel, for  $E_{\text{tot}} = 4.47 \times 10^{40}$  J, the energy of a pure dipole poloidal field with  $B_{1,\max} = 10^{11}$  T), both for  $M_* = 1.4M_\odot$  and  $R_* = 10^4$  m. In the left panel, a dipole (i.e.,  $E_2 = E_3 = 0$ ) deforms the star into an oblate shape. Adding the quadrupole and octupole induces greater ellipticity, and  $\epsilon$  increases monotonically with increasing  $E_2/E_1$  and  $E_3/E_1$  (left-hand panel). If  $E_{\text{tot}}$  is kept constant instead (right-hand panel), we see that  $\epsilon$  decreases as  $E_2/E_{\text{tot}}$  increases and, for a given  $E_2/E_{\text{tot}}$ ,  $\epsilon$  has a maximum when  $E_3/E_{\text{tot}} \approx 0.4(1 - E_2/E_{\text{tot}})$ . The right-hand panel of Fig. 4 shows that increasing  $E_2$  at the expense of  $E_1$  reduces  $\epsilon$ ; in other words, the dipole component (which has the highest energy for a given  $B_{\max}$ ) contributes the most to the magnetic deformation, consistent with Fig. 2.

## 5 DISCUSSION

In this paper, we calculate how the magnetic deformation of a neutron star depends on the orders and relative weightings of the internal magnetic multipoles for a given total magnetic energy. We extend previous calculations (Mastrano et al. 2011; Mastrano & Melatos 2012) to the special case of a quadrupole-poloidal-plus-dipole-toroidal magnetic field, relevant to the poloidal-toroidal twisted torus found by Ciolfi et al. (2009), and to the general case of an arbitrary linear superposition of purely poloidal, axisymmetric multipoles of any order. Our main results are Eqs. (17)–(19), (25), and (26), relating  $\epsilon$  to magnetic field strength, stellar mass and radius, and the relative weightings of the multipoles. We show that, in general,  $\epsilon$  is proportional to energy  $E_{\text{tot}}$ . For single multipoles,  $\epsilon$  decreases with  $l$  to a minimum at  $l = 5$ , then increases monotonically (Fig. 2). We derive a general formula for  $\epsilon$  caused by a superposition of purely poloidal multipoles [Eq. (17)–(19)]. As an explicit example, we calculate  $\epsilon$  for a dipole-quadrupole-octupole field as a function of  $E_1$ ,  $E_2$ , and  $E_3$  [Eq. (25)] and as a function of  $E_2/E_{\text{tot}}$  and  $E_3/E_{\text{tot}}$  [Eq. (26)]. As we see in Eqs. (25)–(26) and in Fig. 4, a purely poloidal field of any multipole order(s) always deforms the star into an oblate shape and  $\epsilon$  increases with  $E_2/E_1$  and  $E_3/E_1$  [Fig. 4 (left)]. On



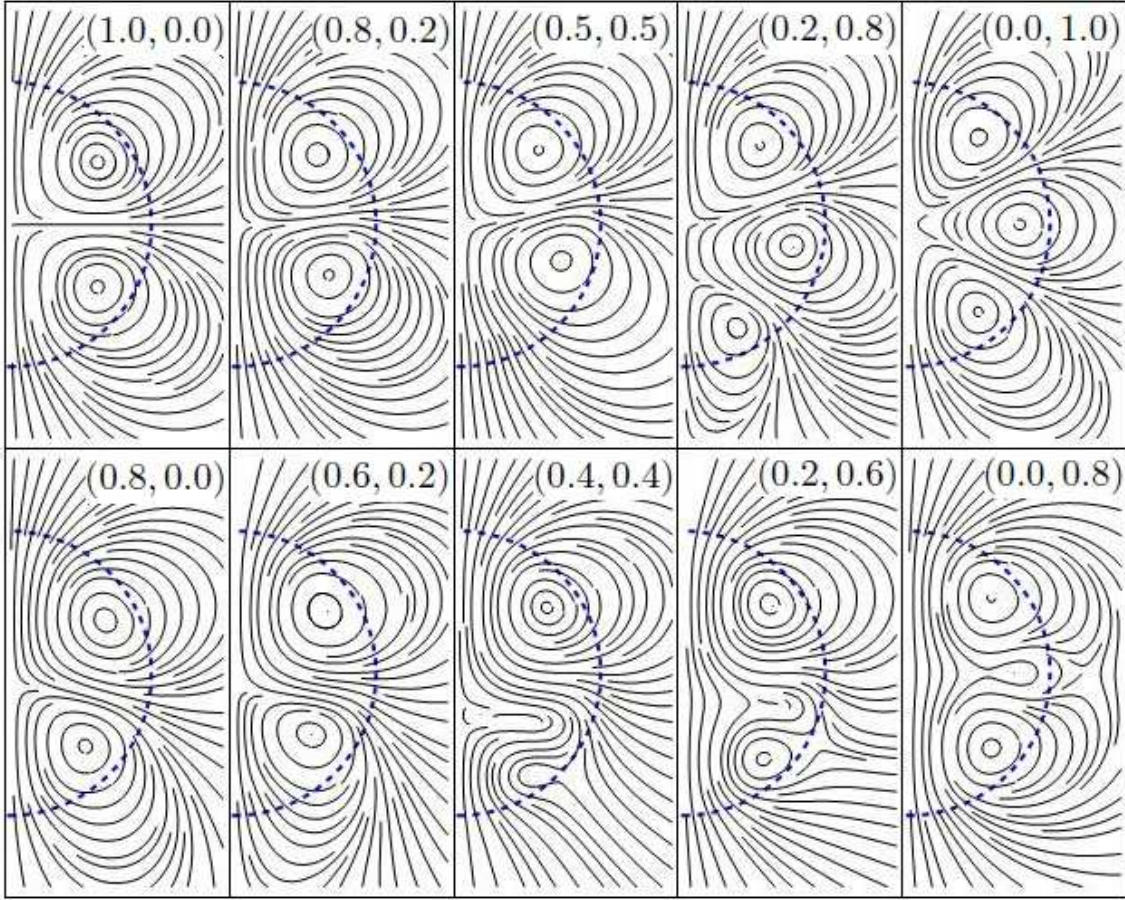


**Figure 3.** Magnetic field lines for a superposition of dipole, quadrupole, and octupole fields with different values of  $(E_2/E_{\text{tot}}, E_3/E_{\text{tot}})$  (label in each panel), where  $E_2$ ,  $E_3$ , and  $E_{\text{tot}}$  are the energies of the quadrupole and octupole components and the total energy respectively. The surface of the star is represented by the blue dashed semicircle. Apparent discontinuities in the field lines are plotting artifacts.

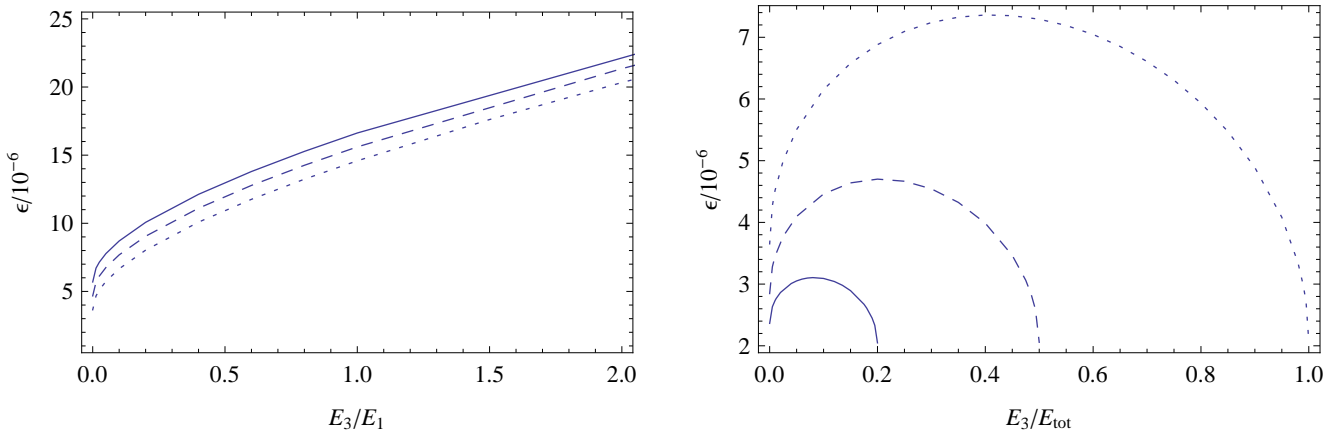


**Figure 4.** Ellipticity  $\epsilon$  (in units of  $10^{-6}$ ) induced by a magnetic field which is a superposition of dipole, quadrupole, and octupole components, as a function of  $E_3/E_1$  (left), the ratio of the energy of the octupole to the dipole, and as a function of  $E_3/E_{\text{tot}}$  (right), the ratio of the energy of the octupole to the total energy. Maximum field strength of the dipole  $B_{1,\text{max}}$  is kept constant at  $10^{11}$  T in the left plot, while total energy is kept constant at  $4.47 \times 10^{40}$  J (the energy of a pure dipole with  $B_{1,\text{max}} = 10^{11}$  T) in the right plot. In the left-hand plot, the three curves correspond to different  $E_2/E_1$  (the ratio of the energy of the quadrupole to the dipole) equal to 0 (dotted curve), 0.5 (dashed curve), and 1.0 (solid curve). In the right-hand plot, the three curves correspond to different  $E_2/E_{\text{tot}}$  (the ratio of the energy of the quadrupole to the total field energy) equal to 0 (dotted curve), 0.5 (dashed curve), and 0.8 (solid curve). Parameters: stellar radius  $10^4$  m, stellar mass  $1.4M_{\odot}$ .

the other hand, for a fixed  $E_{\text{tot}}$ ,  $\epsilon$  decreases as  $E_2/E_{\text{tot}}$  increases and, for a particular  $E_2/E_{\text{tot}}$ ,  $\epsilon$  reaches a maximum when  $E_3/E_{\text{tot}} \approx 0.4(1 - E_2/E_{\text{tot}})$ .

Comparing Eq. (13) to Eq. (7), we see that  $\epsilon$  is smaller for the quadrupole-poloidal-plus-dipole-toroidal field than for the dipole-poloidal-plus-dipole-toroidal field. Eqs. (7) and (13) indicate that a star with purely poloidal magnetic field is always oblate ( $\epsilon > 0$ ). There is, therefore, an upper limit to the ellipticity caused by a purely poloidal field, obtained by setting  $\Lambda = 1$  in Eqs. (7) and (13), but there is no upper limit on the ellipticity of a prolate star ( $\epsilon < 0$ ). In reality, however, there are other limits on  $\Lambda$  (and, hence, an upper limit on  $\epsilon$  for prolate stars) from stability arguments. Akgün et al. (2013) demonstrated analytically the stability of a predominantly toroidal field configuration in a non-barotropic neutron star; for a typical magnetar, with  $B_{1,\text{max}} = 10^{11}$  T, Akgün et al. (2013) found that  $\Lambda \gtrsim 10^{-2}$  is required for stability. Ultimately, however, one needs to conduct time-dependent magnetohydrodynamic simulations to draw convincing conclusions regarding field stability (Braithwaite & Nordlund 2006; Lasky et al. 2011; Ciolfi et al. 2011; Lander & Jones 2012).

X-ray spectra of some magnetars indicate that the surface magnetic field strengths of these magnetars may be greater than the inferred dipole field (Güver, Özel F., & Göğüş 2011; Güver, Göğüş, & Özel 2011). SGR 0418+5729 has an inferred dipole field strength of  $\lesssim 7.5 \times 10^8$  T (Rea et al. 2010), but an analysis of the X-ray spectrum, using the Surface Thermal Emission and Magnetospheric Scattering (STEMS) model (Güver, Özel, Göğüş, & Kouveliotou 2011), concluded that a surface field strength of  $10^{10}$  T fits the data best [see also Tong & Xu (2012) for an alternative explanation]. Güver, Göğüş, & Özel (2011) postulated higher-order multipole(s) at the surface, which fall away with altitude faster than the dipole, to account for the discrepancy. Substituting  $B_{1,\text{max}} = 7.5 \times 10^8$  T into Eq. (7), we find  $\epsilon = 2.05 \times 10^{-10}$  for a star with a purely poloidal dipolar magnetic field structure. Adding a quadrupole component with  $B_{2,\text{max}} = 10^{10}$  T increases  $\epsilon$  to  $1.20 \times 10^{-8}$ ; adding an octupole component with  $B_{3,\text{max}} = 10^{10}$  T raises  $\epsilon$  to  $1.08 \times 10^{-8}$ . While these values of  $\epsilon$  are still too small to generate gravitational waves detectable by current-generation interferometers, the presence of superconducting protons (Mastrano & Melatos 2012; Lander 2013) or quarks (Glampedakis, Jones, & Samuelsson 2012) in the neutron star core can increase  $\epsilon$  by a factor  $\sim H_{c1}/\langle B \rangle$ , where  $H_{c1}$  is the first superconductivity critical field (Glampedakis, Andersson, & Samuelsson 2011) and  $\langle B \rangle$  is the volume-averaged internal field strength. In SGR 0418+5729, a superconducting interior can raise  $\epsilon$  by a factor of 10, increasing the possibility of detection. Hence, any detection of gravitational waves from SGR 0418+5729 will allow us to constrain directly the internal magnetic and material properties of this object. Furthermore, if the orientation of the principal axes of inertia, to be inferred from gravitational wave data, does not match the magnetic inclination angle (the angle between the magnetic and rotation axes), it can be adduced as a compelling evidence for high-order multipoles; as seen in Fig. 3, a superposition of odd and even multipoles is symmetric about the magnetic axis, but not symmetric about the equator.

It is also possible that higher multipoles contribute to the spin down of a newborn magnetar (Thompson, Chang, & Quataert 2004; Metzger et al. 2011; Bucciantini 2012). To generate their strong magnetic fields through a dynamo process, it is hypothesized that magnetars are born rotating fast, with period  $P \lesssim 1$  ms (Thompson & Duncan 1993; Thompson, Chang, & Quataert 2004). Thompson, Chang, & Quataert (2004), Metzger et al. (2011), and Bucciantini (2012) showed how such an object can spin down to  $P \sim 1$  s within  $\sim 10^2$  s. A pure multipole of order  $l$  leads to a spin-down law of the form  $\dot{\Omega} \propto \Omega^{2l+1}$ , where  $\Omega$  is the angular velocity of the star, and one has  $\dot{\Omega} \approx \dot{\Omega}_{\text{dipole}}(R_*\Omega/c)^{2l-2}$ , where  $\dot{\Omega}_{\text{dipole}}$  is the spin-down rate of a pure dipole. For mixed multipoles, the dominant multipole is the one with the strongest  $|\mathbf{B}|$  at the light cylinder  $r = c/\Omega$ , and the spin-down law is some intermediate exponent. For submillisecond newborn magnetars,  $c/\Omega \sim R_*$ , so the contribution of higher multipoles is non-negligible. The gravitational wave energy emitted during this period also makes the newborn magnetar an excellent candidate for a gravitational wave source (Palomba 2001; Stella et al. 2005, 2009; Mastrano et al. 2011). Note that the gravitational waves emitted during this submillisecond phase contribute to the spin-down law as  $\dot{\Omega} \propto \Omega^5$  (Lai, Chernoff, & Cordes 2001; Cutler 2002). This has important implications for gravitational wave searches, since the phase model (which must be known accurately to perform phase-coherent integrations) depends on braking law.

Parfrey, Beloborodov, & Hui (2012a,b) conducted two-dimensional simulations of a rotating, slowly twisting magnetar magnetosphere. They obtained a series of explosive reconnection events and increases in spin-down torque, which can explain the features observed in the 1998 August 27 and the 2004 December 27 giant flares of SGR 1900+14 and SGR 1806–20. Their simulation started from an axisymmetric, north-south-symmetric dipole. As seen in Fig. 3, the addition of quadrupolar and/or octupolar components breaks the hemispherical symmetry, raising the probability of reconnection by complicating the field and simultaneously adding to the reservoir of available magnetic energy. As future work, it will be interesting to ask if a composite  $|l| \leq 3$  field changes the conclusions of Parfrey, Beloborodov, & Hui (2012a,b). If so, then magnetar bursts and giant flares offer another independent way to constrain a magnetar’s magnetic geometry from external observations.

## ACKNOWLEDGMENTS

We thank Arthur Suvorov for discussions. We thank the anonymous reviewer for the constructive comments. Alpha Mastrano thanks Kostas Kokkotas for the hospitality shown during his stay at the University of Tübingen, where this work was com-

pleted. This work is supported by an Australian Research Council Discovery Project Grant (DP110103347) and a University of Melbourne Early Career Researcher Grant.

## REFERENCES

- Abbott B. et al., 2010, *ApJ*, 713, 671  
 Akgün T., Reisenegger A., Mastrano A., and Marchant P., 2013, preprint (arXiv:1302.0273)  
 Arons J., 1993, *ApJ*, 408, 160  
 Arons J., 2000, in Kramer M., Wex N., Wielebinski R., eds., *IAU Colloq. 177: Pulsar Astronomy — 2000 and Beyond*, vol. 202 of *Astronomical Society of the Pacific Conf. Series*, Pulsar Death at an Advanced Age. p.449  
 Barsukov D.P. and Tsygan A.I., 2010, *MNRAS*, 409, 1077  
 Bonazzola S. and Gourgoulhon E., 1996, *A&A*, 312, 675  
 Braithwaite J., 2009, *MNRAS*, 397, 763  
 Braithwaite J. and Nordlund Å., 2006, *A&A*, 450, 1077  
 Braithwaite J. and Spruit H.C., 2006, *A&A*, 450, 1097  
 Bucciantini N., 2012, in Roming P., Kawai N., Pian E., eds., *Death of Massive Stars: Supernovae and Gamma-Ray Bursts*, *Proc. of the IAU Symposium*, vol. 279. p.289  
 Burnett C.R. and Melatos A., 2013, submitted  
 Camilo F., Kaspi V.M., Lyne A.G., Manchester R.N., Bell J.F., D’Amico N., McKay N.P.F., and Crawford F., 2000, *ApJ*, 541, 367  
 Chandrasekhar S., 1956, *Proc. Nat. Acad. Sci.*, 42, 1  
 Chandrasekhar S. and Fermi E., 1953, *ApJ*, 118, 116  
 Chung C.T.Y. and Melatos A., 2011, *MNRAS*, 411, 2471  
 Ciolfi R., Ferrari V., Gualtieri L., and Pons J.A., 2009, *MNRAS*, 397, 913  
 Ciolfi R., Ferrari V., and Gualtieri L., 2010, *MNRAS*, 406, 2540  
 Ciolfi R., Lander S.K., Manca G.M., and Rezzolla L., 2011, *ApJ Lett.*, 736, L6  
 Cutler C., 2002, *Phys. Rev. D*, 66, 084025  
 Dall’Osso S., Shore S.N., and Stella L., 2009, *MNRAS*, 398, 1869  
 Feroci M., Hurley K, Duncan R.C., and Thompson C., 2001, *ApJ*, 549, 1021  
 Ferraro V.C.A., 1954, *ApJ*, 119, 407  
 Gil J. and Mitra D., 2001, *ApJ*, 550, 383  
 Goossens M., 1972, *Ap&SS*, 16, 286  
 Glampedakis K., Andersson N., and Samuelsson L., 2011, *MNRAS*, 410, 805  
 Glampedakis K., Jones D.I., and Samuelsson L., 2012, *PRL*, 109, 081103  
 Gotthelf E.V., Halpern J.P., and Alford J., 2013, *ApJ*, 765, 58  
 Güver T., Göğüş E., and Özel F., 2011, *MNRAS*, 418, 2773  
 Güver T., Özel, and Göğüş E., 2008, *ApJ*, 675, 1499  
 Güver T., Özel F., Göğüş E., and Kouveliotou C., 2007, *ApJ*, 667, L73  
 Katz J.I., 1989, *MNRAS*, 239, 751  
 Haskell B., Samuelsson S., Glampedakis K., and Andersson N., 2008, *MNRAS*, 385, 531  
 Hurley K., Cline T., Mazets E. et al., 1999, *Nature*, 397, 41  
 Ioka K., 2001, *MNRAS*, 327, 639  
 Lai D., Chernoff D.F., and Cordes M., 2001, *ApJ*, 549, 1111  
 Lander S.K., 2013, *PRL*, 110, 071101  
 Lander S.K. and Jones D.I., 2009, *MNRAS*, 395, 2162  
 Lander S.K. and Jones D.I., 2012, *MNRAS*, 424, 482  
 Lasky P.D., Zink B., Kokkotas K.D., and Glampedakis K., 2011, *ApJ Lett*, 735, L20  
 Lyne A.G. and Manchester R.N., 1988, *MNRAS*, 234, 477  
 Lyutikov M., Otte N., and McCann A., 2012, *ApJ*, 754, 33  
 McLaughlin et al., 2003, *ApJ*, 591, L135  
 Markey P. and Tayler R.J., 1973, *MNRAS*, 163, 77  
 Mastrano A. and Melatos A., 2012, *MNRAS*, 421, 760  
 Mastrano A., Melatos A., Reisenegger A., and Akgün T., 2011, *MNRAS*, 417, 2288  
 Medin Z. and Lai D., 2010, *MNRAS*, 406, 1379  
 Melatos A. and Payne D.J.B., 2005, *ApJ*, 623, 1044  
 Metzger B.D., Giannios D., Thompson T.A., Bucciantini N., and Quataert E., 2011, *MNRAS*, 413, 2031

- Nishimura O., 2005, PASJ, 57, 769  
 Palomba C., 2001, A&A, 367, 525  
 Parfrey K., Beloborodov A.M., and Hui L., 2012, MNRAS, 423, 1416  
 Parfrey K., Beloborodov A.M., and Hui L., 2012, ApJ Lett., 754, L12  
 Payne D.J.B. and Melatos A., 2004, MNRAS, 351, 569  
 Pethick C.J., 1992, in Pines D., Tamagaki R., Tsuruta S., eds., The Structure and Evolution of Neutron Stars. Addison-Wesley, New York, p. 115  
 Pitkin M., 2011, MNRAS, 415, 1849  
 Rankin J.M., 1993, ApJ, 405, 285  
 Rea N., 2010, Sci, 330, 944  
 Reisenegger A., 2009, A&A, 499, 557  
 Reisenegger A. and Goldreich P., 1992, ApJ, 395, 240  
 Rezzolla L., Lamb F.K., Marković D., and Shapiro S.L., 2001, Phys. Rev. D, 64, 104013  
 Rezzolla L., Lamb F.K., Marković D., and Shapiro S.L., 2001, Phys. Rev. D, 64, 104014  
 Romani R.W. and Yadigaroglu I.-A., 1995, ApJ, 438, 314  
 Stella L., Dall’Osso S., Israel G.N., and Vecchio A., 2005, ApJ, 634, L165  
 Stella L., Dall’Osso S., Israel G.N., and Vecchio A., 2009, Memorie delle Società Astronomica Italiana, 80, 186  
 Tayler R.J., 1973, MNRAS, 161, 365  
 Thompson T.A., Chang P., and Quataert E., 2004, ApJ, 611, 380  
 Thompson C. and Duncan R.C., 1993, ApJ, 408, 194  
 Thompson C. and Duncan R.C., 2001, ApJ, 561, 980  
 Thompson C., Lyutikov M., and Kulkarni S.R., 2002, ApJ, 574, 332  
 Tong H. and Xu R.X., 2012, ApJ Lett, 757, L10  
 Wright G.A.E., 1973, MNRAS, 162, 339  
 Young M.D., Manchester R.N., Johnston S., 1999, Nat, 400, 848

## APPENDIX A: RADIAL FACTOR OF THE STREAM FUNCTION

Throughout the paper, we postulate that  $f(r)$ , the radial factor of the magnetic field’s separable stream function  $\alpha(r, \theta) = f(r)\Theta(\theta)$ , takes the form of a polynomial in  $r$  with three terms, the minimum needed to fulfill the boundary conditions (ii)–(iv) in Sec. 2.

There is, in fact, no absolute requirement that  $f(r)$  only consists of three terms (nor indeed that it be a polynomial). One can add one or more terms whose coefficients are not fixed by the boundary conditions. This allows one to fine-tune the field to match observations, while keeping the polynomial form of  $f(r)$  to simplify calculations.

As an example, let us examine the case of a purely poloidal dipole field. In Sec. 3.1, we used  $f(r) = (35/8)[r^2 - (6/5)r^4 + (3/7)r^6]$  (Mastrano et al. 2011; Akgün et al. 2013). If we now assume that  $f(r)$  takes the form of  $f(r) = ar^2 + br^4 + cr^6 + dr^5$ , we can reevaluate  $\epsilon$  to find its dependence on  $d$ . We leave  $d$  as a free parameter, then solve for  $a$ ,  $b$ , and  $c$  to match the boundary conditions. We find

$$\epsilon_d = 3.754 \times 10^{-10} \left( \frac{B_{\max}}{10^{11} \text{T}} \right)^2 \left( \frac{M_*}{1.4M_{\odot}} \right)^{-2} \left( \frac{R_*}{10^4 \text{m}} \right)^4 (d^2 + 47.47d + 9.728 \times 10^3), \quad (\text{A1})$$

and the field energy  $E$  is

$$E = 3.247 \times 10^{-4} (d^2 + 81.67 + 5.507 \times 10^3) \frac{\pi B_{1,\max}^2 R_*^3}{\mu_0}. \quad (\text{A2})$$

The energy  $E$  has a minimum at  $d \approx -41$  and  $\epsilon_d$  has a minimum at  $d \approx -24$ .

We plot the field lines for six different values of  $d$  in Fig. A1 [including  $d = 0$  for comparison]. As Fig. A1 shows, the region occupied by the toroidal field (if it is present) expands as  $d$  increases. This raises the possibility of a toroidal field with a relatively weak  $|\mathbf{B}|$  possessing a disproportionately large energy, thereby affecting stability and inferences concerning the SGR burst/giant flare energy reservoir. Fig. A1 shows as well that one can have another neutral curve closer to the origin when  $d$  is large and negative (e.g.,  $d = -50$ ). In theory, a second toroidal field region can exist around this inner neutral curve. These interesting possibilities and calculations will be investigated in a future work.

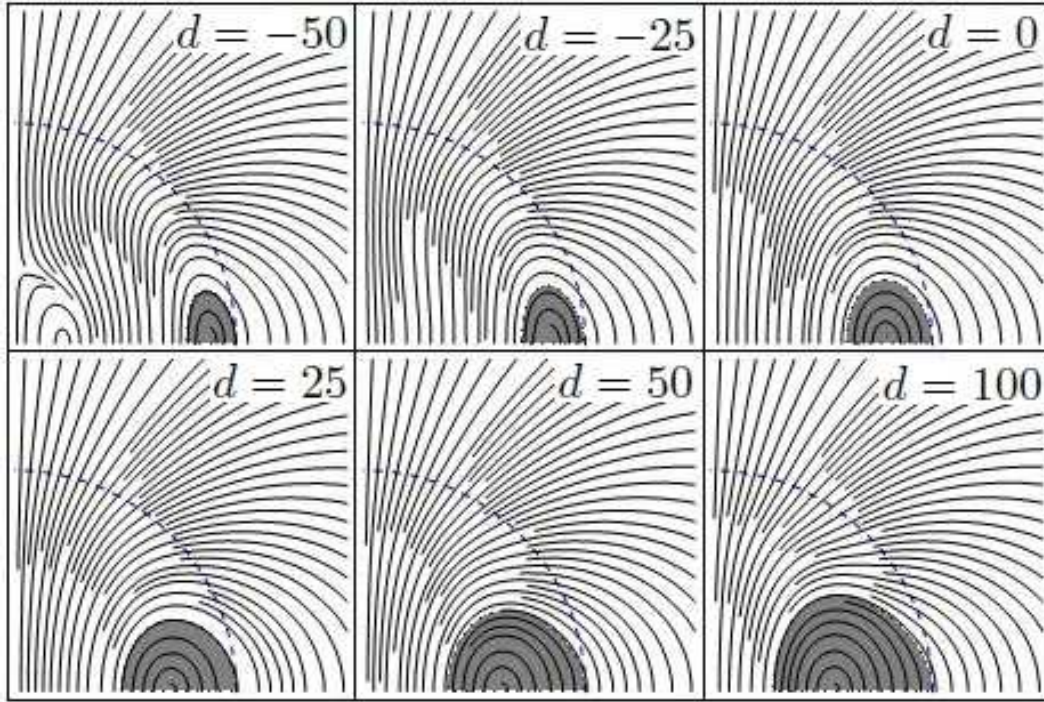


**Figure A1.** Field line plots of the dipole poloidal-plus-toroidal fields, where the radial part of the stream function is  $f(r) = ar^2 + br^4 + cr^6 + dr^5$ , for six different values of the fourth polynomial coefficient  $d$ . The dashed semicircle represents the stellar surface. The toroidal component, if present, is confined to the area around the neutral curves, represented by the shaded region. Apparent discontinuities in the field lines are plotting artifacts.